Nuclear quadrupole resonance in amorphous and crystalline As_2S_3

Mark Rubinstein and P. C. Taylor
Naval Research Laboratory, Washington, D.C. 20375
(Received 25 October 1973)

The pure As^{75} nuclear quadrupole resonances (NQR) of crystalline and amorphous As_2S_3 have been investigated and compared. The temperature dependence of the resonance frequencies, the asymmetry parameters η, and the orientation of the principal axes of the electric field grandient with respect to the crystal axes have been obtained for crystalline As_2S_3 (orpiment). We obtain $\eta_{\rm I} = 0.343$ and $\eta_{\rm II} = 0.374$, where I and II refer to the two inequivalent As sites in the unit cell. A Townes-Dailey calculation for the NQR frequency of the asymmetric AsS_3 pyramidal unit has also been performed. The NQR spectrum of crystalline As_2S_3 consists of two narrow lines approximately 50 kHz wide occuring at 70.38 and 72.86 MHz at 4.2 °K, while the spectrum of amorphous As_2S_3 consists of a broad line with 3.5-MHz halfwidth. This is explained by a distribution of apex pyramidal bonding angles in the glass with a halfwidth of $\sim 1°$. The nuclear transverse relaxation times T_2 have been measured by the spin-echo technique in both the glass and the crystal. In the crystal, $T_2 = 0.6$ msec for site II, and $T_2 \cong 1$ msec for site I; while we obtain $T_2 = 0.6$ msec for the glass. The close agreement between the glass and crystal transverse relaxation indicates the retention of some crystalline correlation in the glass. The spin-lattice relaxation time T_1 has been measured as a function of temperature in the crystal and can be fit by the relation $T_1 = 30.64 \sinh^2(14.5/kT)$, indicating that the nuclei relax by Raman scattering of optical phonons. The spin-lattice relaxation time measured in the glass is much faster, obeying the relation $T_1 = 125T^{-2}$. The faster relaxation in the glass indicates the presence of extra low-frequency modes which are absent in the crystal.

I. INTRODUCTION

The structure of amorphous materials and the nature of the elementary excitations in these substances are both subjects of considerable current interest and debate. X-ray- and neutron-diffraction data on glassy SiO_2 have been variously interpreted as supporting a structural arrangement based either on a random network of SiO_4 tetrahedra[1] or on a more ordered network of conformally distorted regions retaining substantial elements of the crystalline order.[2] The existence of low-frequency modes in amorphous materials, as inferred from specific-heat measurements, has been accounted for by several different models.[3-5] The present paper reports the first application of pure nuclear quadrupole resonance (NQR) to the study of an amorphous material.[6] Specifically, NQR and relaxation results obtained in glassy As_2Se_3 and As_2S_3 are compared with those observed in crystalline As_2S_3, and information is obtained concerning the distribution of bond angles, the extent of crystallinelike order remaining in the glassy state, and the nature of the low-frequency vibrational modes in glasses.

The absence of wave-vector (or crystal-momentum) conservation in amorphous materials makes the interpretation of optical (Raman), x-ray, or neutron scattering experiments much more difficult than in crystalline materials, and information concerning the static and dynamic properties of glasses must therefore be extracted using several different techniques. In addition to scattering experiments, such measurements as infrared and optical absorption, viscosity, and electron microscopy have been profitably employed in the study of vitreous materials. The present NQR results provide another useful tool. NQR can be divided roughly into two areas according to the relative magnitude of the nuclear quadrupole and magnetic dipole interactions. The first area, termed the "high-field" case, arises in those situations where the electric quadrupole interaction is a small perturbation upon the interaction between the nuclear magnetic dipole moment and a large applied magnetic field. The second area, called "pure," "zero-field," or "low-field" quadrupole resonance, arises when the quadrupole interaction, even in the absence of any applied magnetic field, is strong enough to generate resonance frequencies in the radio-frequency range. To the experimentalist, this is more than an academic distinction, since it determines whether a fixed frequency spectrometer may be used in which the external magnetic field is swept to search for the resonance or whether a variable-frequency spectrometer is required. "High-field" NQR has been successfully applied in many vitreous materials to study the nature of the glassy state.[7]

The difficulty in detecting zero-field NQR in glasses is very understandable. The magnitude of the electric field gradient at a nuclear site is an extremely sensitive function of its near-neighbor environment. Since the configuration and position of the nearby atoms vary from site to site in a glass, the over-all linewidth of the resonance is consider-

ably broadened. Taking the results presented in this paper as an example, the halfwidth of the As^{75} NQR observed in crystalline As_2S_3 is ~ 50 kHz, while the resonance halfwidth in glassy As_2S_3 is ~ 3.5 MHz. In As_2Se_3 glass the halfwidth is ~ 6 MHz.

Crystalline As_2S_3, which is a naturally occurring mineral called orpiment, is a yellow layered crystal which can be easily cleaved parallel to the plane of the layers. Vitreous As_2S_3, which may be formed either by heating the crystal above its melting temperature (300 °C) or by heating the appropriate mixture of elemental As and S, is deep red in color, fractures into sharp irregular fragments, and is 8% less dense than the crystalline form. Vitreous As_2S_3 is transparent to light in the near infrared (~ 0.5–10 μm), and windows of pure As_2S_3 glass are manufactured commercially. As_2S_3 is a very stable glass and does not crystallize easily. For these reasons it has been recently studied by many techniques ranging from Raman and infrared spectroscopy to magnetic susceptibility and low-temperature specific heat. The availability of As_2S_3 in both its amorphous and crystalline forms makes this material especially useful for the present study because the information obtained from the As^{75} NQR in the crystal and the glass can be directly compared.

II. BACKGROUND THEORY AND INSTRUMENTATION

In addition to their magnetic dipole moment, nuclei with spin $I \geq 1$ possess an electric quadrupole moment, which can interact with the gradient of any electric field that exists at the nucleus. Such electric field gradients can arise from electrons in the chemical bonds of the atom containing the nucleus, and from charges on nearby atoms or ions. In the presence of an applied magnetic field $\vec{H}$, the Hamiltonian of a nuclear spin with a quadrupole moment Q can be written

$$\mathcal{H} = -\gamma\hbar\vec{H}_0\cdot\vec{I} + \frac{e^2qQ}{4I(2I-1)}[3I_z^2 - I(I+1) + \tfrac{1}{2}\eta(I_+^2 + I_-^2)], \quad (1)$$

where γ is the nuclear gyromagnetic ratio and e is the electronic charge. In Eq. (1), $eq \equiv eq_{zz}$ is the maximum component of the electric-field-gradient (EFG) tensor in the principal-axis system, and the asymmetry parameter η [defined by $\eta = (q_{xx} - q_{yy})/(q_{zz})$] is a measure of the departure of the EFG tensor from axial symmetry.

The As^{75} nucleus is 100% abundant, and has a spin of $I = \frac{3}{2}$. For this case, Eq. (1) predicts the existence of a single resonance line when no external magnetic field is applied to the sample at a resonance frequency[8]

$$\nu = \tfrac{1}{2}(e^2qQ/h)(1 + \tfrac{1}{3}\eta^2)^{1/2}. \quad (2)$$

The quantity e^2qQ/h is known as the "quadrupole-coupling constant," whose theoretical and experimental determination in As_2S_3 and As_2Se_3 will be discussed in Sec. III.

We note there that the coupling constant associated with a single atomic p-state electron which forms an As-S or As-Se covalent bond is of the order of (–) 400 MHz.[9] This large value for the coupling constant per p electron indicates that the nuclear resonance in As_2S_3 and As_2Se_3 will fall into the "low-field" area of quadrupole-resonance phenomena.

A semischematic diagram of the nuclear-resonance spectrometer used in the present study is illustrated in Fig. 1. The NQR spectrometer head is a portable high-power variable-frequency pulsed rf generator which derives its gated dc voltages from the power supply of an Arenberg PG 650-C pulsed oscillator. This head is a modified version of the rf oscillator section of the Arenberg PG 650 and is constructed on a small aluminum chassis. The chassis can be inserted between the poles of an electromagnet when it is necessary to apply a magnetic field to the sample. A peak field of ~ 40-G rf can be achieved in the rotating frame in a 16-mm-diam coil at a frequency of 70 MHz. The spectrometer uses the "spin-echo" method of detecting NQR[10,11] where the radio frequency is applied in the form of short intense pulses, and the transient response of the nuclei following the pulses is observed.

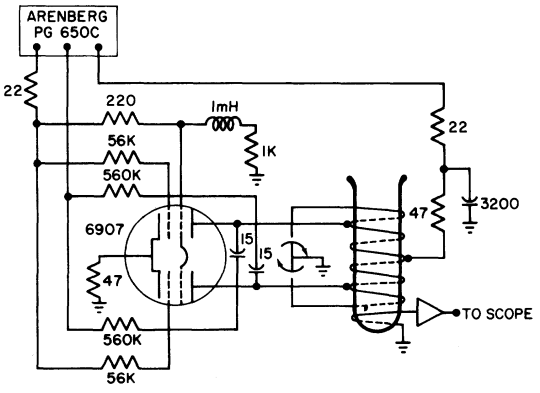

FIG. 1. Semischematic diagram of pulsed NQR spectrometer used in this experiment. Resistance is indicated in Ω, capacitance in pF.

In the spin-echo method, a sequence of two rf pulses is applied with an interval τ between them as shown in Fig. 2. For optimum signal intensity, the second pulse should last twice the duration of the first pulse and the optimum pulse width t is given by the relationship $(\sqrt{3})\gamma ht = \frac{1}{2}\pi$, where h is

FIG. 2. Sequence of rf pulses, decay tails, and spin echoes for optimum echo amplitude.

the magnitude of the rf field pulse in the rotating frame. The application of the first rf pulse at the nuclear resonance frequency results in a transient excitation of the nuclear-spin system, and a free-induction-decay tail may be observed immediately following the pulse. The application of the second pulse at a time τ after the initial pulse, leads to the generation of a responding signal pulse from the spins at time 2τ, a phenomenon known as a "spin echo."[12] Measurements on the amplitude of the spin-echo signal provide the basic experimental technique. The linewidth of the resonance is obtained by measuring the spin-echo amplitude as a function of frequency at a fixed pulse separation. The relaxation time of the transverse component of the nuclear magnetization, or spin-spin relaxation time T_2, is obtained by measuring the decay of the spin-echo amplitude as a function of pulse separation τ. The spin-lattice relaxation time (T_1) may be obtained by observing the decay of the spin-echo signal as a function of repetition rate of the two-pulse sequence.

There are distinct advantages to using the spin-echo method of detecting NQR over the more commonly employed method of continuous-wave detection, especially if the lines are extremely broad as in the case of vitreous As_2S_3 and As_2Se_3. Optimum sensitivity in the cw method is achieved by using field or frequency modulation equal in magnitude to that of the linewidth; and this is impossible to achieve for a very broad line. The degradation of the spin-echo signal by the excessive linewidth is not nearly as severe. Moreover, the spin-echo method gives both the longitudinal and transverse nuclear relaxation times directly.

III. NQR IN CRYSTALLINE As_2S_3

It is necessary to understand the crystalline state NQR in order to interpret better the results found in the glass. Quadrupole resonance in crystalline As_2S_3 (orpiment) was first reported by Pen'kov and Safin[13] who investigated the resonance spectra of orpiment at both room and liquid-nitrogen temperatures, using the pulse-echo method. Two resonances, one from each of the two inequivalent As sites in the unit cell, were found with frequencies of 69.54 and 71.94 MHz, respectively, at 300°K. Pen'kov and Safin also measured the room-temperature nuclear-relaxation behavior of As_2S_3. They did not, however, make measurements using an applied magnetic field, and hence did not determine values for the asymmetry parameter.

We have extended the investigation of Pen'kov and Safin on the NQR of orpiment to include the study of resonance frequencies and relaxation effects at lower temperatures with and without the influence of an externally applied magnetic field. We have also developed a theoretical treatment of the various parameters involved, including the quadrupole-coupling constant, the asymmetry parameter, and the dipolar second moment.

A. Quadrupole-coupling constant

The NQR spectra of orpiment, obtained at room-temperature and at liquid-helium temperature, are displayed in Fig. 3. Natural crystals were used in this study, and identical results were found in crystals originating in several different areas.[14] The spectra were obtained by measuring the amplitude of the As^{75} nuclear spin-echo signal as a function of frequency across the broadened resonance line. Corrections for the frequency variation of the receiver sensitivity were achieved by injecting a pulsed rf reference signal into the pick-up coil of the oscillator tank circuit, and adjusting the amplitude of the reference signal to match that of the spin echo. The amplitude of the reference was then measured and recorded. At room temperature, the signals were repetitively stored in a Nicolet signal-averaging computer to increase the signal-to-noise ratio. At 4.2°K the exceedingly long spin-lattice relaxation time made this technique impractical, and each

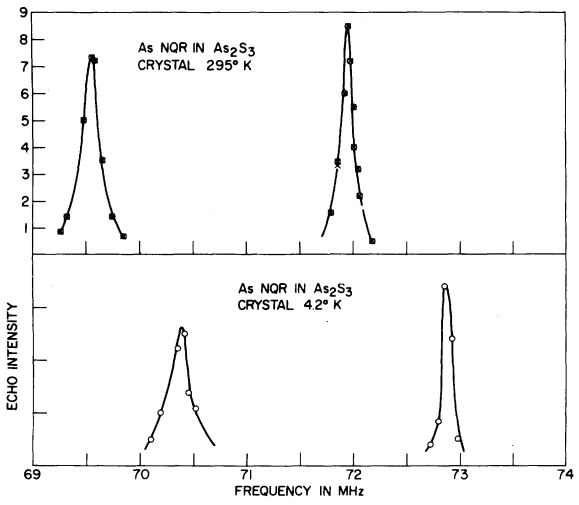

FIG. 3. As^{75} nuclear-quadrupole-resonance spectra of crystalline As_2S_3 at 4.2 and 295°K.

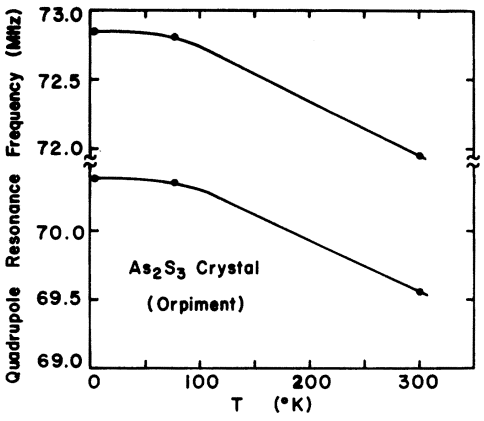

FIG. 4. Temperature dependence of As^{75} resonance frequencies in crystalline As_2S_3. Freehand curves are drawn through the data points.

point was obtained from a single pulse sequence, after which the sample was removed from the liquid-helium Dewar, warmed to room temperature where the nuclei achieved thermal equilibrium with their surroundings, and reimmersed in liquid helium. The process was then repeated at the next frequency.

The NQR spectrum in orpiment consists of a pair of As^{75} resonance lines, one from each of the two inequivalent As sites in the unit cell. At 4.2°K, the nuclear resonance frequencies occur at 70.38 and 72.86 MHz, and decrease with increasing temperature due to the thermal effects of the lattice vibrations.[15] The temperature dependence of the NQR frequencies of the two sites in orpiment is shown in Fig. 4. The room-temperature frequencies agree with those reported by Pen'kov and Safin, but our liquid-nitrogen values are slightly greater than their values. The measured linewidths are all of the order of 50 kHz. As will be shown below, this linewidth cannot be accounted for by dipolar interactions, and it represents a combination of instrumental broadening and broadening caused by inhomogeneities and strains.

The crystal structure of As_2S_3 is monoclinic, although it is nearly orthorhombic since the angle between the a and b crystal axes is 90.5°.[16] The unit cell, projected on the ab plane, is shown in Fig. 5(a). Monoclinic orpiment has a layer structure in which each As atom is covalently bonded to three S atoms in a triangular pyramidal arrangement with an As atom at the apex and three S atoms at the base. The layers are parallel to (010), and held together by weak van der Waals forces. The unit cell consists of eight As atoms and 12 S atoms, but many of these are related by symmetry transformations, and hence have identical quadrupole coupling constants. In fact, there are only two nonequivalent As atoms in the unit cell, giving rise to the two distinct As NQR lines, and these are labeled as I and II in Fig. 5(a).

The x-ray results of Morimoto,[16] coupled with basic chemical-bonding arguments,[17] indicate that linked AsS_3 pyramidal molecules form the basic structural units of the layers in orpiment. There exists much evidence from x-ray diffraction,[2,18] infrared spectroscopy,[19–22] and viscosity measurements[23] that the pyramidal units (as well as the layers) are retained in the glassy state. To a first approximation then, the quadrupole resonance frequencies may be interpreted in terms of isolated AsS_3 pyramids in both the crystal and the glass, which are shown in Fig. 5(b).

The AsS_3 "molecule" contains sp^3 hybridized electron orbitals, of which three form covalent As-S bonding orbitals and the fourth forms an unshared or lone-pair orbital. Each occupied p-elec-

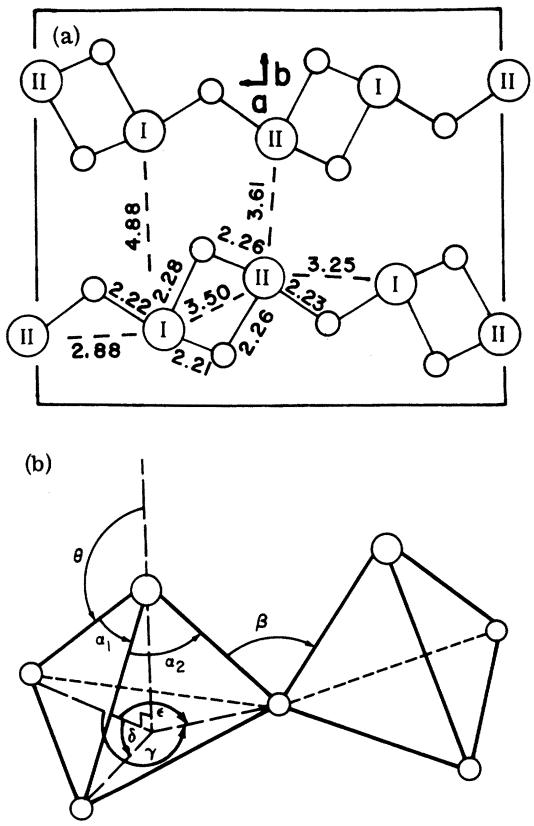

FIG. 5. (a) Unit cell of orpiment (As_2S_3) projected on a (001) plane (ab face). The indicated distances between atoms are in Å. The center of the cell is the inversion point. Small circles denote S atoms (b) The linked AsS_3 pyramidal units of orpiment. Small circles denotes S atoms; large circles denote As atoms.

TABLE I. Eulerian angles [as defined by H. Goldstein, in *Classical Mechanics* (Addison-Wesley, Cambridge, Mass., 1951), p. 107] describing the orientation of the principal axes of the electric-field-gradient tensor with respect to the crystalline axes. The x, y, and z axes of the crystal are taken as the a, c and b axes, respectively.

Site I	Site II
$\Theta = 37°$	$\Theta = 40°$
$\Phi = 149°$	$\Phi = 33°$
$\Psi = 53°$	$\Psi = 128°$

tron As orbital produces an electric field gradient q_p at the As nucleus of magnitude $q_p = e\langle(3\cos^2\theta - 1)/r^3\rangle$. This gradient is modified by the effect of the induced distortion of the inner shell electrons: the Sternheimer antishielding effect. Rather than directly calculate q, Townes and Dailey[24] introduced the concept of the atomic coupling constant $e^2q_{at}Q$, which is the empirically determined quadrupole-coupling constant between the atomic nucleus and a single-orbiting p electron. This has the value $e^2q_{at}Q = -412$ MHz for As^{75}.[9] The molecular quadrupole-coupling constant $e^2q_{mol}Q$ is then evaluated, in the Townes-Dailey approximation, by tensor addition of the contribution of each hybrid p electron to the field gradient. Provided that the nucleus is not situated in a site of cubic symmetry, a finite quadrupole coupling will result.

The theory relating the NQR frequency to the bonding configuration of a *regular* pyramidal molecule is described in the review by Das and Hahn,[8] and results in the following equation:

$$\nu = \frac{e^2q_{at}Q}{2}\left(\frac{(I+1)(1-3\cos^2\theta')}{\sin^2\theta'}\right), \tag{3}$$

where θ' is the angle between the threefold symmetry axis and the As-S bond, and I is the ionic character of the bond.[8] We have extended Eq. (1) to cover the case of an asymmetric pyramidal molecule, which is applicable to As_2S_3. This calculation is presented in the Appendix. Using Eq. (A6), the bond angles and distances given by x-ray data, and an ionic character $I = \frac{1}{2}(X_{AS} - X_S) = 0.25$ (where X_a is the electronegativity of a),[25] the following parameters are calculated for the two nonequivalent sites in orpiment:

$$\nu_I = 117 \text{ MHz}, \quad \eta_I = 0.15;$$

$$\nu_{II} = 114 \text{ MHz}, \quad \eta_{II} = 0.42.$$

Better agreement with the experimentally observed frequencies (72.9 and 70.4 MHz) can perhaps be obtained by taking into account other contributions such as π bonding of the lone-pair orbital. (We have chosen the higher-frequency resonance to be associated with site I, in agreement with the theoretical calculation.) It is clear, however, that most of the field gradient at the As sites is produced by the intrapyramidal hybridized orbitals. The asymmetry parameters are very sensitive to small changes in the bond angles, a fact which must be considered when comparing these values of η to the experimentally determined values to be discussed in Sec. III B.

B. Asymmetry parameter

We have determined an estimate of the asymmetry parameters for sites I and II in crystalline As_2S_3 by measuring the effect of an applied external magnetic field on the NQR spectrum. Zeeman splitting of a pure quadrupole spectrum was first treated by Bersohn[26] using a perturbation procedure. Dean[27] subsequently treated the theory of Zeeman splitting rigorously and discussed the case of $I = \frac{3}{2}$ in detail. The Zeeman field removes the $\pm m$, or the Kramers degeneracy of the quadrupole energy levels, and four lines which are symmetric about the zero-field frequency result. Since the quadrupole coupling constant e^2qQ and the asymmetry parameter η cannot be individually determined in a zero-field experiment for $I = \frac{3}{2}$, it is necessary to apply a small magnetic field. The resulting splittings of the NQR line determine the asymmetry parameter, as well as the orientation of the principal axes of the electric-field-gradient tensor with respect to the crystalline axes.

The Hamiltonian describing the Zeeman splitting of the quadrupole spectrum in the principal-axis system of the electric-field-gradient tensor is given by Eq. (1). The Zeeman portion of this Hamiltonian can be expressed as

$$\mathcal{H}_M = -\Omega(I_z\cos\theta + I_x\sin\theta\cos\varphi + I_y\sin\theta\sin\varphi), \tag{4}$$

where $\Omega = \gamma H_0$ and θ, φ are the polar and azimuthal angles, respectively, for the direction of $\vec{H}_0$ with respect to the Z axis of the EFG. The four resonance frequencies computed from Eq. (1) when $I = \frac{3}{2}$ are

$$\begin{aligned}
\nu_\alpha &= \tfrac{1}{2}e^2qQ(1+\tfrac{1}{3}\eta^2)^{1/2} + (\Delta E_{3/2} + \Delta E_{1/2}),\\
\nu_\beta &= \tfrac{1}{2}e^2qQ(1+\tfrac{1}{3}\eta^2)^{1/2} + (\Delta E_{3/2} - \Delta E_{1/2}),\\
\nu_{\alpha'} &= \tfrac{1}{2}e^2qQ(1+\tfrac{1}{3}\eta^2)^{1/2} - (\Delta E_{3/2} + \Delta E_{1/2}),\\
\nu_{\beta'} &= \tfrac{1}{2}e^2qQ(1+\tfrac{1}{3}\eta^2)^{1/2} - (\Delta E_{3/2} - \Delta E_{1/2}),
\end{aligned} \tag{5}$$

where

$$\Delta E_{3/2} = \frac{\Omega}{2}\left\{\left(1+\frac{2}{\rho}\right)^2\cos^2\theta + \left[\left(1-\frac{1}{\rho}\right)^2 + \frac{\eta^2}{\rho^2} + \frac{2\eta}{\rho}\left(1-\frac{1}{\rho}\right)\cos 2\varphi\right]\sin^2\theta\right\},$$

$$\Delta E_{1/2}=\frac{\Omega}{2}\left\{\left(1-\frac{2}{\rho}\right)^2\cos^2\theta + \left[\left(1+\frac{1}{\rho}\right)^2+\frac{\eta^2}{\rho^2}-\frac{2\eta}{\rho}\left(1+\frac{1}{\rho}\right)\cos 2\varphi\right]\sin^2\theta\right\}\ ,$$

$$\rho^2=1+\tfrac{1}{3}\eta^2.$$

The usual method for determining η consists of mapping out the locus of zero splittings by orienting the crystal in an applied magnetic field. In the present case, this careful procedure is not necessary since the best natural crystals consisted of slightly distorted layers whose principal axes varied $\pm 3°$ to $5°$ over the crystal volume (as determined from Laue x-ray photographs). The small spread in principal-axis directions causes the NQR resonance to broaden in an applied magnetic field, and makes a detailed investigation unprofitable. Instead, the asymmetry in the EFG was obtained by applying the external magnetic field along the three mutually orthogonal $\vec{a}$, $\vec{b}$, and $\vec{c}$ axes. These directions could be ascertained from a visual inspection of the crystal since orpiment cleaves along the *ac* planes, and these planes are striated along the $\vec{a}$ axis. The three spectra, obtained with an applied field of ~875 G are shown in Fig. 6. The frequencies ν_α, ν_β, $\nu_{\alpha'}$, and $\nu_{\beta'}$ are indicated on this figure for sites I and II, respectively, for each direction of the applied magnetic field.

When the magnetic field is applied along the three (mutually perpendicular) principal crystal axes, the following sum rules are obtained using Eq. (5):

$$(\nu_\alpha^a)^2+(\nu_\alpha^b)^2+(\nu_\alpha^c)^2+(\nu_\beta^a)^2 +(\nu_\beta^b)^2+(\nu_\beta^c)^2=(3\gamma H_0/2\pi)^2, \quad (6)$$

$$\nu_\alpha^c\,\nu_\beta^c=\nu_\alpha^a\nu_\beta^a+\nu_\alpha^b\nu_\beta^b.$$

Superscripts in Eq. (6) refer to the crystal axis along which the magnetic field is applied. The frequencies indicated in Fig. 6 obey these sum rules quite well, indicating they can be determined despite the field-induced linewidth. The formulas in Eq. (5) form a set of overdetermined equations for the unknown parameters: the asymmetry constant η and the three Euler angles which determine the orientation of the principal axes with respect to the crystal axes. These parameters, determined by a method of successive approximations, are listed in Table I. The values of η determined for sites I and II are 0.343 and 0.374, respectively.

From the parameters of Table I it can be seen that the principal z axis of the field gradient tensor forms an angle of nearly $40°$ with the b axis which is essentially what one would anticipate from the disposition of the AsS_3 pyramids with respect to the crystal axes. This fact explains why the three traces in Fig. 6 are so similar, since the projection of the z component of the EFG on all three principal crystal axes is substantial.

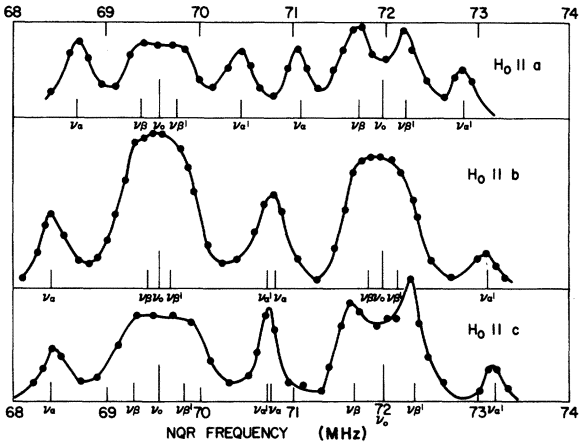

FIG. 6. NQR spectra obtained at room temperature with an applied field of ~875 G applied along the crystal a, b, and c axes, respectively. The zero-field frequencies are indicated by ν_0, 71.94 MHz for site I and 69.54 MHz for site II. ν_α, ν_β, $\nu_{\alpha'}$, and $\nu_{\beta'}$ are the values of the four resonance frequencies obtained with the externally applied magnetic field.

C. Transverse relaxation effects

The nuclear-transverse, or spin-spin, relaxation time T_2 is obtained by measuring the decay of the spin-echo amplitude as a function of pulse separation τ. In a solid T_2 is determined by the dipolar interaction between the nuclear spins and represents the characteristic time with which the nuclei achieve thermal equilibrium with each other. A graph of the spin-echo amplitude as a function of pulse separation, τ, is shown in Fig. 7 for site II of the orpiment crystals at 300°K. The initial decrease of the echo amplitude with τ is Gaussian $\exp[-(2\tau/T_2)^2]$ for small τ. Evidence of an oscillation is seen at $2\tau\approx 1$ msec. At larger values of the pulse separation, a slower, exponential decay seems to be indicated. This behavior is in agreement with that noted by Pen'kov and Safin[13] in their investigation of As_2S_3.

A complete theoretical description of the time evolution of the transverse nuclear magnetization following a spin-echo pulse sequence is not available, but the initial Gaussian decay of the spin echo can be explained by the method of second moments first given by Van Vleck[28] for nuclear-magnetic-resonance linewidths and extended to the broadening of quadrupole spectra by Abragam and Kambe.[29] Abragam and Kambe calculated the second moment $\langle\Delta\omega^2\rangle$ of the NQR line due to the dipole-dipole interactions between both like (resonant) and unlike (nonresonant) neighboring nuclei. For like nuclei

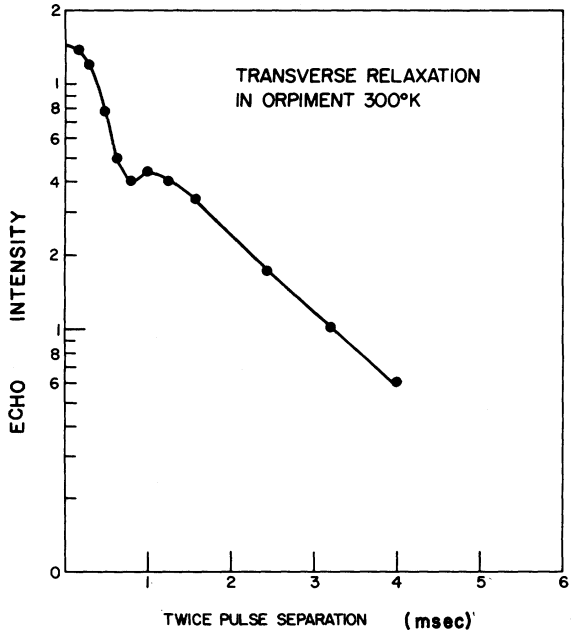

FIG. 7. Echo amplitude of As^{75} in site II of crystalline As_2S_3, following a 90°–180° pulse sequence, as a function of twice the pulse separation. The data were obtained at room temperature with a frequency of 69.5 MHz.

with $I=\frac{3}{2}$, one obtains

$$\langle\Delta\omega^2\rangle=\frac{\gamma^4\hbar^2}{96}\sum\frac{1}{r_{jk}^6}[207(1-3\gamma_{jk}^2)^2 +1512\gamma_{jk}^2(1-\gamma_{jk}^2)+459(1-\gamma_{jk}^2)^2 -108(1-3\gamma_{jk}^2)(\alpha_{jk}^2-\beta_{jk}^2)]. \quad (7)$$

In Eq. (7) the direction cosines of the radius vector $\vec{r}_{jk}$ between nuclei j and k in the principal-axis system are given by α_{jk}, β_{jk}, and γ_{jk}. This equation assumes that the asymmetry parameter is zero. The summation is over like nuclei only.

When applying second-moment calculations to spin-echo phenomena it is necessary to retain only the contribution to the second moment due to resonant nuclei. One must ignore the contribution to the second moment caused by nonresonant neighboring nuclear spins. The resonant spins precess in local fields set up by the nonresonant spins. In lowest order, the contribution to the local field at the resonant spins due to the nonresonant spins is static. Therefore, the contribution of the nonresonant spins is removed in a spin-echo experiment. A criterion determining whether spins are considered resonant is then

$$\Delta\nu<1/t, \quad (8)$$

where $\Delta\nu$ is the resonance frequency differenc between the spins and t is the time duration of the 90° pulse. When this criterion is applied to crystalline As_2S_3, we find all As-I spins are to be considered as mutually resonant, and all As-II spins are mutually resonant, but that no As-I spin is resonant with an As-II spin. Equation (8) will be of importance in Sec. IV where the transverse relaxation of the very broad resonance in the amorphous state is interpreted.

Equation (7) predicts linewidths which are orders of magnitude less than the experimentally determined linewidth of Fig. 3, since random strains and crystal defects are much more effective causes of line broadening than dipolar interactions. However, the second-moment calculation does apply to the transverse relaxation of the spin-echo signal in the limit when the pulse separation τ is small. It can be shown that[30]

$$\langle\Delta\omega^2\rangle=-\frac{d^2\varphi(\tau)}{d\tau^2}\Big|_{\tau=0}\varphi(0)^{-1}, \quad (9)$$

where $\varphi(\tau)$ is the amplitude of the spin-echo signal at pulse separation τ. If $\varphi(2\tau)=\exp[-(2\tau/T_2)^2]$, then

$$T_2=(2/\langle\Delta\omega^2\rangle)^{1/2}. \quad (10)$$

Equations (7) and (10) may be used with the x-ray data to determine the transverse relaxation time expected in crystalline As_2S_3. If the sum is carried out to all like nuclei within a 20-Å sphere, the results for sites I and II are

$$\langle\Delta\omega^2\rangle_{\rm I}=2.2\times10^6, \quad T_2=0.95 \text{ msec}; \quad (11a)$$

$$\langle\Delta\omega^2\rangle_{\rm II}=3.7\times10^6, \quad T_2=0.7 \text{ msec}. \quad (11b)$$

The initial decay of the experimental spin-echo signal in Fig. 7 for site II is Gaussian with a relaxation time $T_2=0.6$ msec. Similar results were obtained for site I ($T_2\approx1$ msec). The agreement between the calculated and experimental transverse relaxation times is sufficient to conclude that the dominant contributions to the relaxation in crystalline As_2S_3 are the dipolar effects.

At somewhat larger values of τ an oscillation is observed in the transverse relaxation of As_2S_3. This oscillatory behavior is nearly what one would expect from the Zeeman splitting of the As^{75} quadrupole resonance by the earth's magnetic field.[11,31] However, when the sample is shielded from the earth's field by placing the spectrometer in a mu-metal box, no alteration of the oscillatory behavior is observed. It is therefore concluded that the oscillations are an intrinsic phenomenon, similar to the oscillations first observed in the free-induction decay of CaF_2 by Lowe and Norberg.[32]

At longer times the decay of Fig. 7 becomes exponential (Lorentzian) with a characteristic relaxation time of ~1 msec for both site I and site II. If the Lorentzian and Gaussian portions of the curve

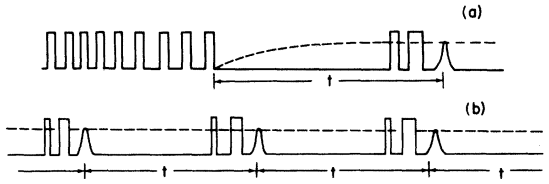

FIG. 8. (a) Saturating comb pulse sequence for measuring T_1. (b) Repetition rate pulse sequence for measuring T_1.

are due to independent mechanisms, then the initial intensity of the Lorentzian decay is approximately 30% of the total intensity.

The interpretation of the Lorentzian component is uncertain, although the oscillatory behavior of the spin-echo amplitude, and the evolution from Gaussian decay at short times to exponential decay at long times, have been observed in other materials. This behavior has been noted, for example, in the nuclear relaxation of ferromagnetic cobalt[33] and in the transverse nuclear quadrupole relaxation of K_2PtCl_6.[34] In the case of cobalt, Shaw attributes these effects to microscopic, inhomogeneous broadening, and presents a detailed theoretical description of the case of spin-spin coupling via the Suhl-Nakamura interaction. The applicability of this explanation to the situation in orpiment is uncertain.

D. Spin-lattice relaxation

Spin-lattice relaxation is the process by which the magnetization of an ensemble of nuclei approaches its thermal equilibrium value following a perturbing influence such as a pulse of rf energy. Interactions between the nuclear spin system and the low-energy excitations of the solid (phonons) are responsible for spin-lattice relaxation in crystalline materials. Thus, a study of spin-lattice relaxation in orpiment provides information concerning details of the phonon spectrum.

The As^{75} nuclear spin-lattice relaxation rates were measured using two different techniques. In the first technique [Fig. 8(a)], a saturating comb of 90° rf pulses is initially applied to the crystal. At a time t after the termination of the saturating comb, an interrogating 90° –180° pulse sequence whose separation is less than T_2 is applied. The amplitude of the resulting spin echo is proportional to $1-e^{-t/T_1}$, where T_1 is the spin-lattice relaxation time. The second technique, illustrated in Fig. 8(b), uses a 90° –180° pulse sequence (with pulse separation less than T_2), which is periodically repeated after an interval t. It may be shown[35] that the steady-state echo signal is again proportional to $1-e^{-t/T_1}$. The validity conditions for this technique are discussed elsewhere.[35] Good agreement was obtained between the two methods of measuring spin-lattice relaxation.

The spin-lattice relaxation time T_1 is obtained by plotting the unsaturated echo height minus the echo height at time t after the termination of the saturating comb of 90° pulses on semilog paper, and by noting the time at which the resulting curve decreases to e^{-1} of its initial value. This curve, obtained from data on the lower frequency line of orpiment at 77 °K, is shown in Fig. 9. The expected exponential decay of the nuclear magnetization with time is found at 297, 77, and 4.2 °K. The spin-lattice relaxation times obtained at these three temperatures are displayed in Table II, along with the values obtained in previous investigations.[13,36] The relaxation time of orpiment at 4.2 °K was so long (~ 2 h) that it was necessary to warm the sample to room temperature between each measurement to avoid saturation by the previous pulse sequence.

Quadrupole nuclear spin-lattice relaxation results primarily from first-order Raman processes involving the inelastic scattering of a phonon by the spin system.[37] The relaxation can proceed via either acoustical[37] or optical[34,38] phonons. When a single optical mode dominates the relaxation process, the temperature dependence of the relaxation time is given by[38]

$$T_1 = A \sinh^2(\epsilon/2kT), \tag{12}$$

where ϵ is the phonon energy and A is a proportionality constant.

As shown in Fig. 10, the data for orpiment are best fit with $A = 30.64$ sec and $\epsilon = 29$ °K, which corresponds to an optical lattice vibration of frequency 20 cm^{-1}. The lowest optical phonons in orpiment, as determined by Raman spectroscopy, lie at 25

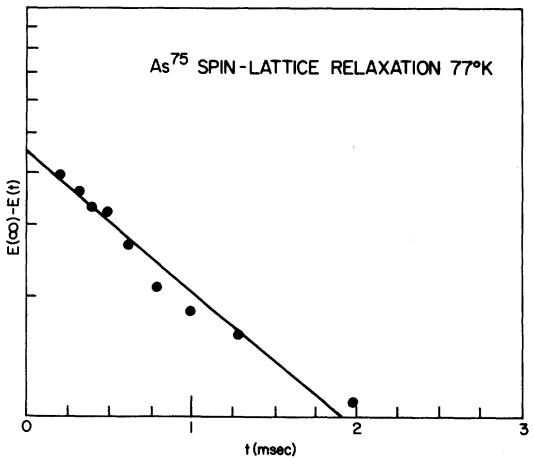

FIG. 9. Spin-lattice relaxation of crystalline As_2S_3 at 77 °K.

TABLE II. Spin-lattice relaxation times in orpiment.

Temp. (°K)	T_1 (sec)
4.2	7.4×10^{3}
77	1.1, (0.3)[a]
297	3.2×10^{-2}, (3.3×10^{-2})[b]

[a]Reference 13. [b]Reference 36.

and 35 cm^{-1},[17,21,39] and have been attributed to rigid layer vibrations.[17,40] The fit to the temperature dependence of the T_1 data is in reasonable agreement with the Raman data. The deviation from the theoretical curve in Fig. 10 near 300°K probably results from the influence of higher-lying optical phonons.

IV. NQR IN AMORPHOUS As_2S_3 AND As_2Se_3

Despite numerous investigations concerning the structure of glassy As_2S_3 and As_2Se_3, the subject is still a matter of considerable debate. The proposed structural models for As_2S_3 and As_2Se_3 glasses fall into two categories: those that are based on a continuous three-dimensional random network of well-defined AsS_3 or $AsSe_3$ pyramidal units[22,41] and those that invoke two-dimensional layerlike correlations between pyramidal units such as exist in the crystal modifications.[19,42]

X-ray and neutron-diffraction results on these two glasses have been discussed using these two somewhat disparate interpretations. Hopkins *et al.*[43] deduced from their x-ray diffraction study that order barely extends beyond the AsS_3 structural unit; Konnert *et al.*[2] interpret their neutron-diffraction results as indicating that the local structure of As_2Se_3 glass looks very much like crystalline layered As_2Se_3 out to at least 20 Å, while Leadbetter *et al.*[44] deduce a correlation length of 10 Å in glassy As_2Se_3. X-ray studies by Porai-Koshits and Vaipolin[45] are interpreted as indicating that the sheet structure is retained, but that it is distorted and cross linked at various points. Tsuchihashi and Kawamoto[46] also conclude that the structure of As_2S_3 glass is a layer structure similar to that of orpiment, but with a distorted and open structure. In a recently published x-ray diffraction study, Renninger and Averbach[47] state that their results do not support the existence of As_2Se_3 layers in As_2Se_3 glass.

The existence of strong covalent bonding within the layers, and the much weaker bonding between layers, in crystalline As_2S_3 and As_2Se_3 makes it reasonable that a layer structure could be maintained in the glassy state. The relatively low glass transition temperatures (T_g = 187 and 212°C in As_2Se_3 and As_2S_3, respectively) have been interpreted as reflecting the breakup of the weak van der Waals forces between the layers while the break in the slope of the viscosity curves, which occurs at considerably higher temperatures, has been attributed to the breakup of the layers themselves.[48,49] Optical properties in the 1–14-eV range[50,51] and in the infrared region[19,42] provide supporting evidence for the existence of layerlike correlations in glassy As_2S_3 and As_2Se_3, even in the liquid phase. Our NQR results in vitreous As_2S_3 and As_2Se_3 are best interpreted by assuming that layers are still retained in the amorphous phases of these materials. Although we have indicated a lack of unanimity on this point, it seems to us to be the most reasonable conclusion in light of the available evidence. Moreover, this conclusion is supported by our measurements of the spin-spin relaxation in the amorphous state of As_2S_3, which shows a great similarity to the spin-spin relaxation of the crystalline material. As will be discussed in Sec. IV B, this indicates that the local environments of the As nuclei in the crystalline and the glassy state of As_2S_3 are quite similar.

A. Quadrupole-coupling constant

The As^{75} NQR spin-echo spectrum of amorphous As_2S_3 is shown in Fig. 11 where the spectrum of

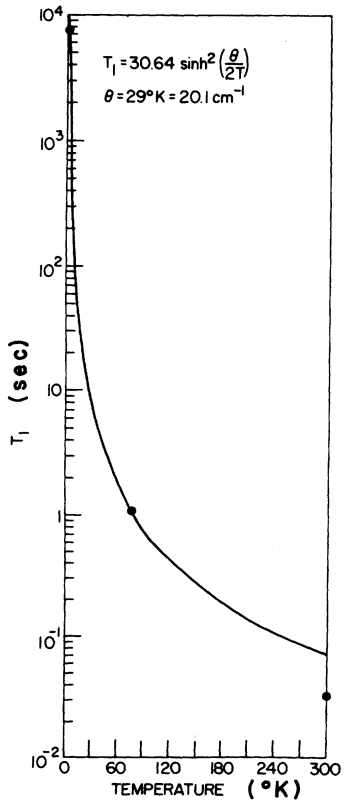

FIG. 10. Spin-lattice relaxation times in crystalline As_2S_3 as a function of temperature. The three points are the experimental data, and the line is a fit to theory.

crystalline As_2S_3 is also displayed for comparison. The data were obtained by measuring the intensity of the spin-echo signal as a function of frequency across the inhomogeneously broadened resonance line. The NQR spectrum of crystalline As_2S_3 consists of two narrow lines approximately 50 kHz wide, but in glassy As_2S_3 the spectrum consists of a single extremely broad line of approximately 3.5-MHz halfwidth at $1/e$. The glass line, whose center is located about midway between the two crystalline lines, is presumably itself composed of two lines, one from each of the two inequivalent As sites in the unit cell. The transverse-relaxation (T_2) results in glassy As_2S_3, to be described below, support this contention. The width of the line is caused by a distribution in the EFG due to bond angle distortions present in the glass.

Vitreous As_2Se_3, which is based on a crystalline material isomorphic to crystalline As_2S_3, also displays a broad spectrum located near 60 MHz as shown in Fig. 12. The vertical lines in Fig. 12 indicate the position of the resonances in crystalline As_2Se_3 as reported by Kravchenko *et al.*[38] at 300 °K.

The NQR linewidth in the glasses is primarily due to deviations in the apex bonding angles (α_i of Fig. 5) of the AsS_3 and $AsSe_3$ pyramidal units. In As_2S_3 we estimate the magnitudes of these deviations in α by comparing the width of the glass line to the frequencies of the two As sites in the crystal for which the apex angles are known from x-ray data. The average apex bonding angle of the first As site in crystalline orpiment exceeds that of the second by 1.3°. A difference in NQR frequencies of 2.48 MHz is observed between these two sites. If

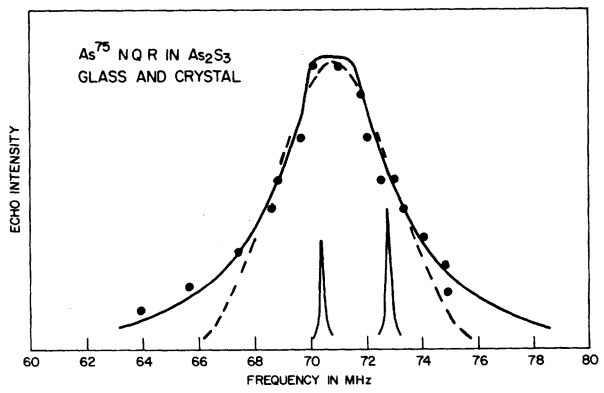

FIG. 11. Nuclear-quadrupole-resonance spectrum of vitreous As_2S_3 at 4.2 °K. The experimental data are shown by the points. The solid and dashed lines are fits to the data by Lorentzian and Gaussian distributions, respectively, of resonance frequencies. The spectrum of crystalline As_2S_3 is also displayed for purposes of comparison.

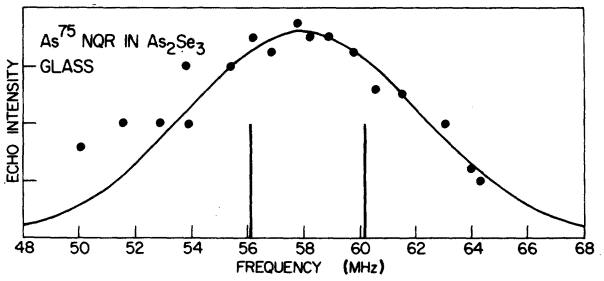

FIG. 12. NQR spectrum of vitreous As_2Se_3 at 4.2 °K. The vertical lines indicate the resonance frequencies of crystalline As_2Se_3.

the spread in frequencies is assumed to vary linearly with α over the region of interest, then one may extrapolate to the NQR data of vitreous As_2S_3.

Since the transverse relaxation-time measurements to be discussed in Sec. IV B indicate the two inequivalent As sites of the crystal remain in the glass, we assume two Gaussian distributions of equal width and fit the data of Fig. 11 (dashed line). The data are fit by two Gaussians of halfwidths at $1/e$ of 2.0 MHz separated by 2.0 MHz (dashed line of Fig. 11). A halfwidth of 2.0 MHz corresponds to a distribution of average apex bonding angles for the two sites in the glass of approximately 1.1°.

The data of Fig. 11 can also be approximated by assuming two Lorentzian lines (solid line of Fig. 11), separated by 1.9 MHz, whose halfwidths at half-height are 1.4 MHz. This fit corresponds to a distribution of average apex bond angles for each site whose halfwidth is 0.75°.

A third estimate of the average apex-bond-angle deviations in the glass can be obtained by using Eq. (3), which assumes that $\eta = 0$, and by calculating the best fit to the spectrum assuming two Gaussian distributions of average apex bonding angles α [which can be easily related to the angle θ' of Eq. (3)]. The resulting distributions in frequency are slightly skewed to the low-frequency side but are very nearly Gaussian. This method yields an average halfwidth at $1/e$ for the average apex bond angle of each glass site of 0.6°. Although the exact number for the distribution of average apex bond angles in glassy As_2S_3 varies somewhat (0.6° to 1.1°) depending on the method of estimation, the obvious fact which emerges is that the pyramidal units are very well defined.

Similar calculations for crystalline and glassy As_2Se_3 can be performed with the result that the deviation of average apex bond angles is on the order of ±3° in glassy As_2Se_3. The data for glassy As_2Se_3 as presented in Fig. 12 are not accurate enough to warrant the fitting procedures discussed for glassy As_2S_3, and the solid line through the data

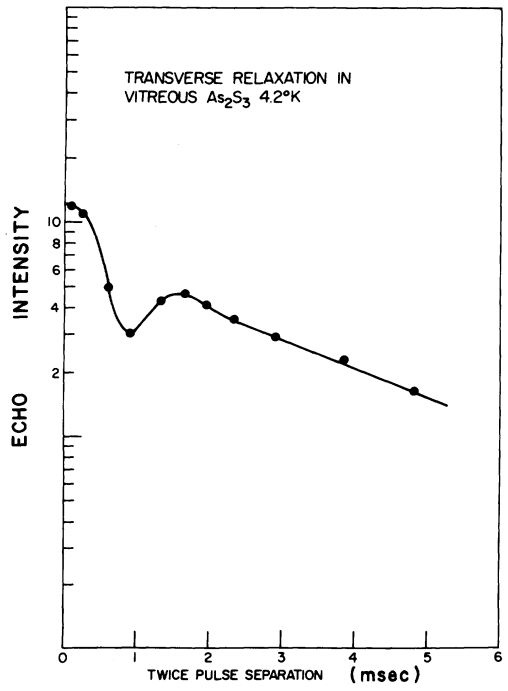

FIG. 13. Transverse relaxation of amorphous As_2S_3 at 70.75 MHz. The echo decay is plotted as a function of twice the pulse separation.

points in Fig. 12 represents two Gaussian curves of 4.5-MHz halfwidths, separated by 4 MHz. Although the glassy $AsSe_3$ pyramidal units are more distorted than the AsS_3 units, the average apex angles of the two inequivalent pyramids in crystalline As_2Se_3 differ more than in crystalline As_2S_3.[18]

B. Transverse-relaxation effects

The transverse-relaxation measurements in vitreous As_2S_3 were obtained using the same procedure as described above for crystalline As_2S_3 with the exception that they were performed on a sample at 4.2°K at 70.75 MHz. The results were independent of frequency within experimental error. As in the crystalline case, the initial decay is Gaussian $(e^{(-2\tau/T_2)^2}$, where τ is the pulse separation), with a transverse relaxation time $T_2 = 0.6$ msec as shown in Fig. 13. The asymptotic behavior at long times, where the decay appears to be exponential, is different from that observed in orpiment (compare Figs. 7 and 13). The asymptotic slope in the glass is approximately a factor of 2 less than in either of the two sites in the crystal, and corresponds to a relaxation time of ~3 msec if the exponential and Gauusian decays are due to independent mechanisms. The decay curve of Fig. 13 is independent of the frequency at which the measurement was performed.

The results of the second-moment calculation for crystalline As_2S_3 reveal that approximately half the contribution to the second moment is due to the nearest-neighbor resonant As nuclei (second-nearest-neighbor As nuclei), and the dipolar fields from second- and third-nearest resonant neighbors are responsible for most of the remainder. The transverse-relaxation time, to which the second moment calculation is intimately related, is therefore useful in obtaining information on the near-neighbor environment. From the near equality of the crystalline and amorphous initial relaxation behavior, we conclude that the near-neighbor environments of the crystal and the glass are quite similar. Specifically, these results argue for the existence in the glass of the two inequivalent As atoms in the crystalline unit cell, and also for the retention in the glass of the two-dimensional correlations between AsS_3 pyramidal units which exist in the crystalline phase.

As discussed in Sec. IIIC, only the interactions between mutually resonant nuclei are effective in contributing to transverse relaxation as measured by the spin-echo technique. In this context, mutually resonant nuclei refer to those interacting nuclear spins that are simultaneously flipped by the applied rf pulse. With a pulse duration of ~7 μsec, only nuclei whose resonance frequencies are within ~150 kHz of each other can be considered mutually resonant, according to Eq. (8). The distinction between the effects of resonant and nonresonant nuclei on the spin-echo transverse relaxation time can be seen in the data of Mestagh *et al.*[52] on the proton relaxation time of zeolite. In that work, the T_2 obtained from the echo is compared to the T_2 obtained from the slope of the free-induction-decay signal and from the value of cw linewidth, and found to be an order of magnitude longer than either of these. Since there is no inhomogeneous broadening in this system, the discrepancy is due to the differing effects of the nonresonant Al nuclei upon the transverse relaxation time measured by the different techniques.

Two criteria must be satisfied in order for the transverse-relaxation times in the crystal and the glass to be nearly equal. First the number of first, second and third-nearest-neighbor *resonant* nuclei must be essentially the same in the two materials. This means that the two As sites in the crystal must be preserved on the average in the glass. For the pulse width used, near-neighbor nuclei in the glass must have quadrupole-resonance frequencies within $\Delta\nu \sim 1/t \sim 150$ kHz in order to be mutually resonant. Thus even though the two As sites in the glass have resonance frequencies which vary by $\Delta\nu \sim 1.5$ MHz (Sec. IV A) throughout the bulk sample, the variance locally is nearly always ten times less than this spread. This fact implies, of course, that on the average the shift in frequency

of nuclei in the glass corresponding to site I in the crystal is not great enough to overlap the frequency of nearest-neighbor nuclei corresponding to site II. In terms of the variation of average apex bond angles discussed in Sec. IV A, this restriction implies that on the average near-neighbor like As nuclei (which are in fact second-nearest neighbors within a layer) have average apex bond angles differing by no more than 0.1° even though the total deviation in the bulk sample is on the order of 1°.

The second criterion which must be satisfied in order for the transverse-relaxation times of the crystal and the glass to be nearly equal is that near-neighbor resonant nuclei must be separated by approximately the same distances in both materials. This fact, coupled with the preservation of the two inequivalent As sites in the glass, strongly suggests that the two-dimensional correlations between AsS_3 pyramidal units which exist in the crystal are by and large present in the glass.

Until now, we have been discussing the distribution of S-As-S apex angles [α_1, α_2, and α_3 of Fig. 5(b)], while the random-network model is concerned with the distribution of the As-S-As bonding angles [β of Fig. 5(b)]. The random-network model, as applied to As_2S_3 and As_2Se_3 glass in its simplest form, postulates the existence of a random distribution of As-S-As bond angles (β), with no variation whatsoever in the S-As-S pyramidal apex angles. However, the T_2 data on glassy and crystalline As_2S_3 are not consistent with such a model.

Since only resonant nuclei contribute to the spin-echo transverse relaxation, a model of the vitreous state of As_2S_3 which postulates a completely random and uncorrelated distribution of β-type bonding angles would result in an initial spin-spin relaxation time in the glassy state ~ 10 times longer than the initial spin-spin relaxation time in the crystalline state for the experimental parameters used in this study—a prediction which is at variance with what is actually observed. (The factor of 10 is obtained from the ratio of the NQR linewidth in the glass to the amplitude of the applied rf field.) Thus, even if we assume that a distribution of As-S-As bonding angles contributes to the distribution of resonance frequencies implied by the NQR spectrum of vitreous As_2S_3 (Fig. 11), we must still conclude that these angles are correlated as in the crystal.

The transverse-relaxation measurements in glassy As_2S_3 support structural models which invoke the preservation of layerlike correlations between pyramidal units and are at variance with models invoking a continuous random network of pyramidal units. There is significant short-range structural order remaining in the amorphous state of As_2S_3.

C. Spin-lattice relaxation

Measurements of the specific-heat,[53,54] thermal conductivity,[53,54] acoustic attenuation,[55,56] far infrared and microwave absorption,[57,58] and Raman scattering[41,59] of glasses at low temperatures have indicated the existence of an enhanced density of very-low-frequency vibrational modes which appear to be characteristic of the amorphous state. At temperatures above 1°K, a large excess heat capacity is found in glasses upon comparing them to crystalline forms of the same substance; this excess heat capacity (which is proportional to T^3) has been attributed to optical modes of very low frequency which are intrinsic to the glassy state.[60] At temperatures below 1°K a contribution to the specific heat which varies linearly with temperature has been discovered in a variety of glasses.[53,54] It has quite recently been proposed that this anomalous specific heat may arise from a distribution of localized defects, present in amorphous solids, in which tunneling between two near equilibrium positions can occur.[5,61]

This model, hereafter termed the AHVP model after its originators,[5,61] postulates that a certain number of atoms or groups of atoms have two equilibrium positions described by an asymmetric double-well potential. Transitions between the two positions are possible by tunneling, whereby a resonant phonon is absorbed or emitted. The linear temperature dependence of the specific heat is then explained by AHVP by postulating that the two-level systems must have a constant distribution of level spacings ΔE, which remains finite and continuous in the vicinity of $\Delta E = 0$. The total number of such levels with $\Delta E < kT$ is then proportional to T, leading to a specific heat likewise proportional to T.

The AHVP theory has received some independent experimental confirmation by the recent discovery that the acoustic attenuation of 1-GHz sound waves in vitreous silica is strongly dependent on the acoustic amplitude at temperatures below 0.5°K.[55,56] A large increase in attenuation is observed as the incident acoustic intensity is decreased. Such an effect is in accord with the AHVP model, since the resonant absorption of sound by the localized two-level systems saturates, and can be observed only if the sound amplitude is extremely small. Since nuclear spin-lattice relaxation proceeds via vibrational modes, and since the vibrational spectrum appears to be significantly altered by the disappearance of crystalline order, it may be anticipated that the nuclear spin-lattice relaxation of vitreous As_2S_3 will differ markedly from that of crystalline As_2S_3. Comparison of the spin-lattice relaxation of the crystalline and amorphous states makes it possible to verify the existence of an enhanced density of low-frequency

modes in the amorphous state by a new and independent technique.

Increased nuclear spin-lattice relaxation rates may be a general feature of disordered materials. Greatly increased spin-lattice relaxation rates have been observed for protons in organic glasses as compared to the rates in crystalline counterparts.[62–64] Whether the relaxation proceeds via a Raman process as in most crystalline materials or via a direct process, these measurements indicate an enhanced density of low-frequency modes in the organic glasses. A similar increase in the relaxation rate of B^{11} in glassy B_2O_3 over the crystalline material has also been observed.[65] Finally, the present measurements of the temperature dependence of As^{75} spin-lattice relaxation in glassy and crystalline As_2S_3 indicate an enhanced density of low-frequency modes in the vitreous material.

The As^{75} nuclear spin-lattice relaxation in amorphous As_2S_3 has been investigated using both the saturating comb and the pulse-repetition-rate techniques described above (Sec. IIID, Fig. 8). The resulting relaxation curve at a sample temperature of 4.2 °K is shown in Fig. 14 where circles and triangles represent measurements taken using the repetition rate and saturating comb techniques, respectively. One difference between spin-lattice relaxation in the amorphous material and the crystal, which is immediately apparent from this figure, is that the decay cannot be represented by a single exponential characterized by one relaxation time. A second difference is the rate of decay, which is ~15 sec to reach $1/e$ in the glass compared to ~2 h in the crystal.

In crystalline materials the measured relaxation is characterized by two competing processes—direct interaction of nuclei with the phonons (T_1 processes) and interactions between nuclear spins (T_2, spectral or spin diffusion processes). Spin-diffusion processes are effectively removed in crystals by completely saturating the nuclear spin system with the rf pulses. However, the measurement of T_1 in amorphous As_2S_3 involves considerations which were not important in the measurements of crystalline As_2S_3. The glass linewidth is 3.5 MHz, while the crystal linewidth is 50 kHz. It is not possible, therefore, to saturate the entire NQR line in the amorphous state by applying a train of rf pulses. With the available rf power we are only capable of "burning a hole" in the broad resonance line. Under these conditions it is conceivable that the nuclear spin system can lose its excitation energy by spectral or spin diffusion to nearby nonresonant spins, instead of directly to the lattice via spin-lattice relaxation. Such a process would render comparisons between the crystal and the glass meaningless since different physical phenomena would be involved.

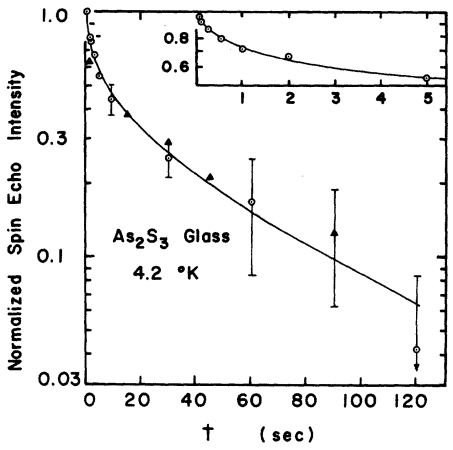

FIG. 14. Normalized spin-echo intensity $[E(\infty)-E(t)/E(\infty)]$ vs time (twice the 90°–180° pulse separation) for vitreous As_2S_3 at 4.2 °K. Circles represent T_1 data taken with repetition rate technique; triangles, T_1 data taken with saturating comb technique.

The weight of evidence indicates that spectral diffusion is not a significant factor in the relaxation of the nuclear excitation in the glass and that direct spin-lattice relaxation is the dominant process. Spectral diffusion can occur when a fraction of the spins are selectively excited by an rf pulse; the excitation may spread out to unexcited spins with different resonant frequencies through spin-spin coupling. This mechanism leads to an apparent loss of excitation at the frequency of measurement, but does not involve the lattice. Hence it is expected to be temperature independent. We have observed, a strong dependence of relaxation rate on temperature, which indicates that spectral diffusion is unimportant. Moreover, there is no indication of spectral diffusion from the previously discussed T_2 measurements. The effect of diffusion is to cause the spin echo to decay as $e^{-kt^3/3}$, where k is the probability of spectral diffusion.[66] Such behavior is not observed, and is further evidence for the lack of spectral diffusion. The spin lattice relaxation is also unaffected by changing the duration of the saturating comb of rf pulses illustrated in Fig. 8 which again indicates the absence of spectral diffusion in the amorphous state. Finally, when two oscillators are employed at slightly different frequencies, there is no effect at one frequency upon saturating the line at the second frequency. If spectral diffusion were important, one would expect some saturation to occur at the measurement frequency due to saturated spins diffusing from a nearby frequency.

The spin-lattice relaxation behavior of amorphous As_2S_3 at 77 °K is shown on a semilog plot in

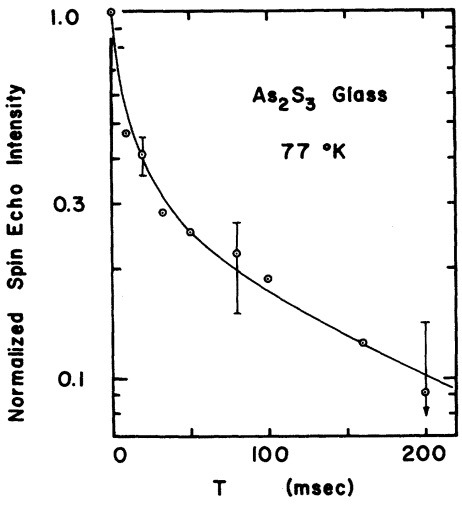

FIG. 15. Normalized spin-echo intensity vs time (twice the 90°–180° pulse separation) for vitreous As_2S_3 at 77 °K.

Fig. 15. It has the same characteristic shape as at 4.2 °K (Fig. 14), but the relaxation at 77 °K is much faster. We interpret the nonlinear decay curves of Figs. 14 and 15 in terms of a continuous distribution of relaxation times resulting from the disorder intrinsic to the amorphous state.

The models proposed to explain the anomalous low-temperature thermal properties of amorphous materials fall into two general categories—those which invoke atomic tunneling between two near-equilibrium positions,[5,61] and those which assume low-frequency vibrational modes which obey Bose statistics.[3,53] With either type of model one can obtain a distribution of relaxation times which would yield nonlinear decay curves. In the tunneling models, the magnitude of the spin-lattice relaxation depends on the relaxation time of a two-level state to the phonons τ_c as will be indicated below. A distribution of nuclear spin lattice relaxation times results from a distribution in τ_c's. In the models which assume low-frequency vibrational modes which obey Bose statistics, one obtains a distribution of relaxation times if the vibrational states are to some extent localized and vary from region to region in the glass.

One may still define a characteristic relaxation time for the glass as the time for the nuclear spin system to attain $(1 - 1/e)$ of its equilibrium magnetization after the application of a saturating comb of rf pulses (i. e., the time at which the decay curves of Figs. 14 and 15 fall to $1/e$). This definition is particularly meaningful because the shape of the decay curves is independent of temperature, as will be demonstrated below.

The temperature dependence of an effective T_1, as defined above, in glassy As_2S_3 is presented in Fig. 16. The effective relaxation rate T_1^{-1} is proportional to T^2 from 77 to 1.1 °K and can be described fairly accurately by the empirical relation

$$T_1 = 125T^{-2}. \tag{13}$$

The relaxation rates in crystalline As_2S_3 and glassy As_2Se_3 are also plotted in Fig. 16 for comparison. The effective spin-lattice relaxation rate $(1/T_1)$ measured in As_2S_3 glass is much greater than the relaxation rate in the crystals at any given temperature, and this difference is enhanced at lower temperatures where the crystal relaxation rate decreases exponentially with temperature, while the glass relaxation rate remains proportional to T^2.

In a crystalline material, a T^2 dependence of the relaxation rate occurs whenever the dominant modes relaxing the nuclear spins are at energies which correspond to temperatures lower than the measurement temperatures. The T^2 temperature dependence in glassy As_2S_3 is strong evidence for the existence of very-low-frequency vibrational modes in the glass which are thermally excited even at ~ 1 °K, and are strongly coupled to the nuclear spins.

It is informative to divide out the T^2 temperature dependence of the relaxation curves in glassy As_2S_3 to determine if the shape of the curve is otherwise invariant. Figure 17 plots the decay curves at 4.2, 14.8, and 77 °K as a function of T^2t. The data taken at all three temperatures fall on a universal curve, whose shape is determined by a temperature-independent distribution of relaxation centers. The maximum and minimum re-

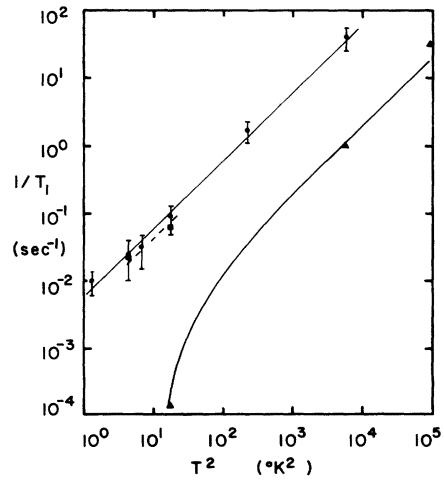

FIG. 16. Relaxation rate $(1/T_1)$ vs temperature squared for vitreous As_2S_3 (circles), crystalline As_2S_3 (triangles), and vitreous As_2Se_3 (squares).

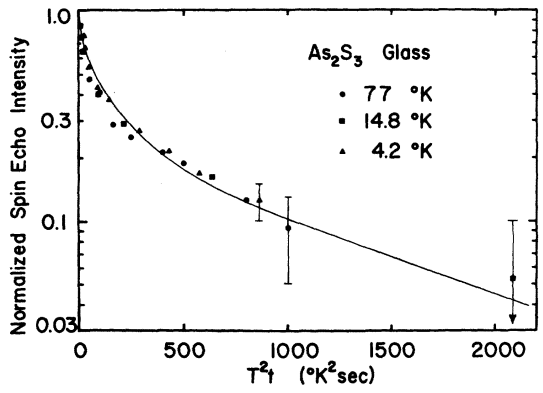

FIG. 17. Normalized spin-lattice decay for vitreous As_2S_3 taken at 4.2, 14.8, and 77 °K vs T^2t, where T is temperature and t is the time. The solid line is a theoretical fit to the data as described in the text.

laxation rates, as given by the maximum and minimum slopes of the curve, differ by a factor of ~ 100. Since the distribution of relaxation rates is governed by the slope of the decay curve, all relaxation rates in the distribution have the same T^2 temperature dependence.

Although the relaxation rates in amorphous materials are generally much faster than in corresponding crystalline materials, not all vitreous materials show a T^2 temperature dependence. In organic glasses the proton spin-lattice relaxation is proportional to T^2 in O-terphenyl + 20% xylene from 4.2 to 77 °K, while it appears to be proportional to $T^{1.5}$ in O-terphenyl and O-terphenyl + 20% benzene over this same temperature range.[64] However, one does not observe a temperature dependence of the relaxation rate stronger than T^2 as one does in crystalline materials whenever the measurement temperature falls below the characteristic temperature of the modes effective in relaxing the nuclear spins. All relaxation measurements in glassy materials to date point to interactions with low-frequency modes.

Spin-lattice relaxation of Si^{29} in glassy SiO_2 has also been reported at 300 °K.[67] Since Si^{29} is only 1% naturally abundant and has no quadrupole moment, its relaxation rate is considerably slower than that of As^{75} in As_2S_3 (10 h at 10 kG and 1.1 min in the earths magnetic field); these long relaxation times would make any measurements at low temperatures in vitreous SiO_2 extremely difficult, which is unfortunate because the low-frequency modes in this material are, at present, the most thoroughly studied.

Before attempting to apply specific models for the low-frequency modes to the nuclear spin-lattice relaxation of amorphous As_2S_3, there are two points which can be made without recourse to calculation. First, the much faster relaxation of the glass vis-a-vis the crystal indicates the existence of an enhanced density of low-frequency modes in the glass. Second, the nonexponential decay is evidence of a distribution of relaxation times due to a corresponding distribution of mode frequencies or of mode relaxation rates. Any quantitative analysis of the spin-lattice relaxation behavior in amorphous As_2S_3 is at best an order of magnitude estimate because even the number of atoms participating in these low-frequency modes is unknown. Nonetheless, we conclude with two calculations of the number of modes necessary to give the observed relaxation rates in glassy As_2S_3 assuming first that the modes are two-level tunneling states (AHVP model) and second that the modes are harmonic oscillator modes spacially localized due to inhomogeneities in the glass structure.

Relaxation via two level localized states should follow in form relaxation via spin-$\frac{1}{2}$ paramagnetic impurities[55] with the modification that the interaction is by modulation of the electric field gradient instead of the magnetic field. As in the case of relaxation via paramagnetic impurities, reasonable nuclear spin-lattice relaxation rates are obtained only if the relaxation is assumed to proceed by nuclear spin diffusion processes (outside of a small region of radius r_0 surrounding the two level state) and not by the direct interaction of the localized two level state with the nuclear spins.

We assume the existence of two nearby potential minima such that an atom or group of atoms can tunnel through the energy barrier separating these two equilibrium positions. A Boltzmann distribution between the localized states is established by resonant absorption or emission of single phonons or by a two-phonon Raman process. The characteristic relaxation time τ for tunneling from one equilibrium position to the other due to such one- and two-phonon processes can be obtained by ultrasonic attenuation measurements.[68] Such measurements have been performed by Ng and Sladek[69] on amorphous As_2S_3, and they obtain $\tau \sim 10^{-5}$ sec at 2 °K.

The usual approach to spin-lattice relaxation follows the classical work of Bloembergen, Purcell, and Pound.[70] The nuclear spin Hamiltonian is divided into a secular part ($\mathcal{H}_0$) and a fluctuating nonsecular perturbation ($\mathcal{H}_1$). One calculates the transition probabilities between the states of $\mathcal{H}_0$ induced by the perturbation $\mathcal{H}_1$. When the time dependence of $\mathcal{H}_1$ can be described by a single correlation time τ, the theory gives the well known result which may be applied to a nucleus adjacent to a tunneling defect

$$1/T_L \sim [\tau/(\omega_0^2\tau^2+1)]\omega_1^2, \tag{14}$$

where ω_0 ($\sim 2\pi \times 70$ MHz) and ω_1 are typical frequencies of $\mathcal{H}_0$ and $\mathcal{H}_1$, respectively, and τ is the relaxation time of the two level state ($\sim 10^{-5}$ sec).

Only nuclei near the two-level state are relaxed directly, but the more distant As nuclei can relax to the tunneling defect by nuclear spin diffusion that occurs through the mutual spin flips between neighboring nuclear spins, in a manner similar to nuclear relaxation caused by fixed paramagnetic impurities in solids. Assuming rapid diffusion, the average relaxation time T_1^{av} will be given by

$$T_1^{av} \approx T_L/c, \tag{15}$$

where c is the concentration of tunneling defects.[71]

Since $\omega_0\tau \sim 10^2 \gg 1$ in Eq. (14), one obtains for the average relaxation time

$$T_1^{av} \approx (\omega_0/\omega_1)^2 \tau/c. \tag{16}$$

The concentration of two-level states can be obtained from the magnitude of the linear term in the specific heat of As_2S_3, and has been determined by Stephens[54] as $c \sim 2\times 10^{-5}$ tunneling states per °K per As nucleus. An upper bound on the frequency associated with the perturbation ω_1 is the linewidth of the resonance line in the glass ($\omega_1 < 2\pi \times 7$ MHz). With this maximum value, $\omega_0/\omega_1 \gtrsim 10$ and Eq. (16) yields

$$T_1^{av} \gtrsim 50 \text{ sec}, \tag{17}$$

which is consistent with the average relaxation times observed in glassy As_2S_3 at low temperatures (T_1 is between 10 and 100 sec for temperatures between 4.2 and 1.1 °K).

One possible difficulty with this estimate is that the very effect which creates the large fluctuating field gradient of magnitude ω_1 may violate a necessary criterion for the occurrence of spin diffusion processes. That is, it may be energetically impossible for the nuclear spin surrounding a two-level state with large ω_1 to interact via spin diffusion processes. If this restriction is valid, then the predicted average relaxation time can be orders of magnitude greater than that indicated by the NQR experiments.

In the above calculation, the temperature dependence of T_1 is proportional to the temperature dependence of τ. For $kT \gg \epsilon$ where ϵ is the energy difference between the two lowest states of the double well potential, the temperature dependence of τ is $\tau \propto T^{-1}$ for a one-phonon process[68] and $\tau \propto T^{-2}$ for a two-phonon Raman process.[72] Sussmann[72] has shown that Raman processes predominate over direct processes above a critical temperature, which is consistent with the observed T^{-2} dependence of the spin-lattice relaxation in glassy As_2S_3.

Some authors have attributed the low-temperature specific-heat anomaly in glasses to the existence of low-frequency modes of the harmonic oscillator type.[3,53] Assuming that the number of these modes per unit energy remains finite and constant as the mode energy ϵ approaches zero, (an assumption which is necessary to account for the linear variation of the specific heat with temperature at low temperatures) it is possible to account for the observed distribution of spin-lattice relaxation times shown in Fig. 16, and to estimate the expected relaxation times at low temperatures.

We utilize the same theory as discussed earlier for crystalline As_2S_3 (i.e., nuclear relaxation through Raman scattering of optical phonons.) In the high-temperature limit, where $kT \gg \epsilon$, the relaxation rate $T_1(\epsilon)$ of nuclear spins to a single optical phonon of energy ϵ may be written

$$1/T_1(\epsilon) = AN_0^2 k^2 T^2/\epsilon^4, \tag{18}$$

where A is a proportionality constant, N_0 is the constant density of low-frequency modes, and the energy denominator takes explicit account of the energy dependence of the transition matrix elements according to Van Kranendonk's theory.[37]

The intensity decay curve for a distribution of relaxation rates can be expressed as a sum over volume elements within which there exist given densities of localized modes. If all low-frequency modes are localized to roughly the same extent, and the relaxation in any given region of the glass is dominated by modes at a given energy ϵ, then the expression for the decay in intensity becomes

$$I(t,\ T) \propto \int_0^{\epsilon_{max}} e^{-t/T_1(T)} d\epsilon, \tag{19}$$

where ϵ_{max} is the maximum phonon energy in the constant distribution of modes effective in relaxing the nuclear spins. An upper bound on ϵ_{max} is the lowest measurement temperature at which one observes a T^2 temperature dependence for the nuclear spin-lattice relaxation rate.

With T_1 from Eq. (18), the integral of Eq. (19) can be easily evaluated. The solid line in Fig. 17 is the theoretical fit to the experimental data where the asymptotic behavior at long times has been fit by a suitable value of the adjustable parameter $C = AN_0^2 \epsilon_{max}^{-4}$.

A crude estimate of N_0 can be obtained from the value of C necessary to fit the data. If one assumes (i) that the value of A necessary to fit the relaxation rate in crystalline As_2S_3 in the high-temperature approximation is appropriate to the low-frequency modes in the glass, (ii) that there is one oscillator per unit cell in the crystalline mode, and (iii) that $\epsilon_{max} \sim 1$ °K, then $N_0 \sim 10^{-4}$ modes per AsS_3 group per °K. Although this number is an order of magnitude greater than the density predicted from specific-heat measurements, it represents an upper bound imposed by the experimental limitations. If ϵ_{max} is assumed to be 0.3 °K (i.e.,

if the T^2 temperature dependence in Fig. 2 exists down to 0.3 °K), then the estimated value of N becomes $\sim 10^{-5}$.

To distinguish between the two proposed relaxation mechanisms—relaxation via the two-level tunneling states of the AHVP model or relaxation via low-frequency localized harmonic-oscillator modes—careful measurements in the temperature range from 1 to 0.1 °K are needed. In addition, ultrasonic attenuation measurements in crystalline and glassy As_2S_3 are indicated to determine if there is a nonsaturating component in the glassy material, as would be expected if there is a substantial density of low-frequency harmonic-oscillator modes.

V. SUMMARY

We have used the technique of nuclear-quadrupole-resonance spectroscopy to investigate the amorphous state of As_2S_3 and As_2Se_3. The availability of crystalline As_2S_3 (orpiment) proved very useful, since comparisons between the crystalline and the amorphous state could be made. By comparing the linewidths of crystalline and glassy As_2S_3, we have concluded that a distribution of pyramidal apex bonding angles exists in the glass, with a halfwidth of approximately 1°.

The similarity between the transverse relaxation times of crystalline and glassy As_2S_3 shows that the glass retains elements of crystalline correlations.

On the other hand, we have found the spin-lattice relaxation of the crystal and the glass to differ both in magnitude and temperature dependence. We attribute this to the presence of extra low-frequency vibrations in the glass which are absent in the crystal.

ACKNOWLEDGMENTS

We wish to thank Dr. G. H. Stauss for deriving the asymmetry parameters of orpiment from the data and Dr. J. Lewis for programming the T_2 calculation.

APPENDIX

The neutral As atom has a valence-electron configuration of $4s^2 4p^3$. According to the principles of molecular bonding, these electrons reside in sp^3 hybrid orbitals, whose lobes are directed along the As-S bond, or in orthogonal "lone-pair" orbitals. The wave function describing these directed orbitals may be written[73]

$$\begin{aligned}
&S\varphi_s + (1-S^2)^{1/2}[a\varphi_z + b\varphi_x + (1-a^2-b^2)^{1/2}\varphi_y],\\
&S_1\varphi_s + (1-S_1^2)^{1/2}(\varphi_z\cos\theta - \varphi_x\sin\theta),\\
&S_2\varphi_s + (1-S_2^2)^{1/2}(\varphi_z\cos\theta - \varphi_x\sin\theta\cos\delta\\
&\qquad - \varphi_y\sin\theta\sin\delta),\\
&S_3\varphi_3 + (1-S_3^2)^{1/2}(\varphi_z\cos\theta - \varphi_x\sin\theta\cos\gamma\\
&\qquad - \varphi_y\sin\theta\sin\gamma).
\end{aligned} \tag{A1}$$

The angles of Eq. (A1) are shown in Fig. 5(b). Orthogonalization of these wave functions yields the following six equations in the six unknowns S, S_1, S_2, S_3, a, and b:

$$\begin{aligned}
&SS_1 + (1-S^2)^{1/2}(1-S_1^2)^{1/2}(a\cos\theta - b\sin\theta) = 0,\\
&SS_2 + (1-S^2)^{1/2}(1-S_2^2)^{1/2}[a\cos\theta - b\sin\theta\cos\delta\\
&\qquad - (1-a^2-b^2)^{1/2}(\sin\theta\sin\delta)] = 0,\\
&SS_3 + (1-S^2)^{1/2}[a\cos\theta - b\sin\theta\cos\gamma\\
&\qquad + (1-a^2-b^2)^{1/2}(\sin\theta\sin\gamma)] = 0,\\
&S_1S_2 + (1-S_1^2)^{1/2}(1-S_2^2)^{1/2}(\cos^2\theta + \sin^2\theta\cos\delta) = 0,\\
&S_1S_3 + (1-S_1^2)^{1/2}(1-S_3^2)^{1/2}(\cos^3\theta + \sin^2\theta\cos\gamma) = 0,\\
&S_2S_3 + (1-S_2^2)^{1/2}(1-S_3^2)^{1/2}[\cos^2\theta + \sin^2\theta\cos\\
&\qquad \times(\delta-\gamma)] = 0.
\end{aligned} \tag{A2}$$

By introducing the new parameters $u_1 = S_1/(1-S_1^2)^{1/2}$, $u_2 = S_2/(1-S_2^2)^{1/2}$, $u_3 = S_3/(1-S_3^2)^{1/2}$, and $u = S/(1-S^2)^{1/2}$ the latter three equations may be solved:

$$\begin{aligned}
u_1^2 &= -\left(\frac{\cos^2\theta + \sin^2\theta\cos\gamma}{\cos^2\theta + \sin^2\theta\cos\epsilon}\right)(\cos^2\theta + \sin^2\theta\cos\delta),\\
u_2^2 &= -\left(\frac{\cos^2\theta + \sin^2\theta\cos\delta}{\cos^2\theta + \sin^2\theta\cos\gamma}\right)(\cos^2\theta + \sin^2\theta\cos\epsilon),\\
u_3^2 &= -\left(\frac{\cos^2\theta + \sin^2\theta\cos\epsilon}{\cos^2\theta + \sin^2\theta\cos\delta}\right)(\cos^2\theta + \sin^2\theta\cos\gamma).
\end{aligned} \tag{A3}$$

We define the variables x and y by the relations $x = a/(1-a^2-b^2)^{1/2}$ and $y = b/(1-a^2-b^2)^{1/2}$, and solve the remaining three equations in terms of the new variables. We obtain

$$\begin{aligned}
y &= \frac{(1-u_3/u_1)\sin\delta - [1-(u_2/u_1)\sin\gamma]}{(1-u_3/u_1)(u_2/u_1-\cos\delta) - (1-u_2/u_1)(u_3/u_1-\cos\gamma)},\\
x &= \frac{(u_3/u_1-\cos\gamma)\sin\delta - (u_2/u_1-\cos\delta)\sin\gamma}{(u_3/u_1-\cos\gamma)(1-u_2/u_1) - (u_2/u_1-\cos\delta)(1-u_3/u_1)} + \cos\theta,\\
u &= [(b\sin\theta - a\cos\theta)u_1]^{-1} = \frac{1+x^2+y^2}{u_1(y\sin\theta - x\cos\theta)}.
\end{aligned} \tag{A4}$$

With the wave functions expressed in terms of the asymmetrical pyramid it is now necessary to calculate the electric-field-gradient tensor produced by each occupied orbital, sum the contributions of the five orbitals involved, and diagonalize the resulting matrix. This process is facilitated by using the Wigner-Eckart theorem to calculate the electric-field-gradient tensor q_{jk}:

$$q_{jk} = -\tfrac{1}{2}q[\tfrac{3}{2}(l_j l_k + l_k l_j) - \delta_{jk} l(l+1)]. \tag{A5}$$

In Eq. (A5), the orbital angular-momentum operators l_i operate within the $L=1$ manifold of the p electron states, since the s electrons are spherically symmetric and produce no electric field gradient at the As nucleus. The electric-field-gradient tensor is then formed by evaluating the sum of the matrix elements of q_{jk} for each of the occupied orbitals in the AsS_3 molecule—two electrons in the lone-pair orbital, and one in each of the three bonding orbitals. The resulting 3×3 matrix becomes

$$\begin{aligned}
q_{xx} &= (1-S_1^2)(\sin^2\theta - \tfrac{1}{2}\cos^2\theta) + (1-S_2^2)[\sin^2\theta(\sin^2\delta - \tfrac{1}{2}\cos^2\delta) - \tfrac{1}{2}\cos^2\theta] + (1-S_3^2)[\sin^2\theta(\sin^2\gamma - \tfrac{1}{2}\cos^2\gamma) - \tfrac{1}{2}\cos^2\theta] \\
&\quad + (1-S^2)(3b^2-1), \\
q_{xy} &= \tfrac{3}{2}(1-S_2^2)\sin^2\theta(\sin\delta\cos\delta) + \tfrac{3}{2}(1-S_3^2)\sin^2\theta(\sin\gamma\cos\gamma) + 3(1-S^2)b(1-a^2-b^2)^{1/2}, \\
q_{xz} &= -\tfrac{3}{2}(1-S_1^2)\cos\theta\sin\theta + \tfrac{3}{2}(1-S_2^2)\cos\theta\sin\theta\sin\delta + \tfrac{3}{2}(1-S_3^2)\cos\theta\sin\theta\sin\gamma + 3(1-S^2)ab, \\
q_{yy} &= +(1-S_1^2)(-\tfrac{1}{2}) + (1-S_2^2)[\sin^2\theta(\cos^2\delta - \tfrac{1}{2}\sin^2\delta) - \tfrac{1}{2}\cos^2\theta] \\
&\quad + (1-S_3^2)[\sin^2\theta(\cos^2\gamma - \tfrac{1}{2}\sin^2\gamma) - \tfrac{1}{2}\cos^2\theta] + (1-S^2)(2-3a^2-3b^2), \\
q_{yz} &= \tfrac{3}{2}(1-S_2^2)\cos\theta\sin\theta\cos\delta + \tfrac{3}{2}(1-S_3^2)\cos\theta\sin\theta\cos\gamma + 3(1-S^2)a(1-a^2-b^2)^{1/2}, \\
q_{zz} &= (1-S_1^2)(\cos^2\theta - \tfrac{1}{2}\sin^2\theta) + (1-S_2^2)(\cos^2\theta - \tfrac{1}{2}\sin^2\theta) + (1-S_3^2)(\cos^2\theta - \tfrac{1}{2}\sin^2\theta) + (1-S^2)(3a^2-1).
\end{aligned} \tag{A6}$$

When the matrix is transformed (by computer), to a set of principal axes X, Y, and Z with diagonal components q_{XX}, q_{YY}, q_{ZZ}, then the NQR frequency is given by

$$\nu = \tfrac{1}{2}e^2 qQ(1+\tfrac{1}{3}\eta^2)^{1/2}, \tag{A7}$$

where $q = q_{ZZ}$ and $\eta = (q_{XX} - q_{YY})/q_{ZZ}$.

[1] B. E. Warren, Kristallogr. 16, 1264 (1971) [Sov. Phys.-Crystallogr. 16, 1106 (1972)].
[2] J. H. Konnert, J. Karle, and G. A. Ferguson, Science 179, 177 (1973).
[3] H. B. Rosenstock, J. Non-Cryst. Solids 7, 123 (1972).
[4] P. Fulde and H. Wagner, Phys. Rev. Lett. 27, 1280 (1971).
[5] P. W. Anderson, B. I. Halperin, and C. M. Varma, Philos. Mag. 25, 1 (1972).
[6] M. Rubinstein and P. C. Taylor, Phys. Rev. Lett. 29, 119 (1972).
[7] See, for example, P. J. Bray, in *Magnetic Resonance*, edited by C. K. Coogan *et al.* (Plenum, New York, 1970).
[8] T. P. Das and E. L. Hahn, *Solid State Physics*, edited by F. Seitz and D. Turnbull (Academic, New York, 1958), Suppl. 1.
[9] E. Schempp and P. J. Bray, in *Physical Chemistry*, edited by D. Henderson (Academic, New York, 1970), Vol. IV.
[10] E. L. Hahn and B. Herzog, Phys. Rev. 93, 639 (1954).
[11] B. Herzog and E. L. Hahn, Phys. Rev. 103, 148 (1956).
[12] See, for example, G. E. Pake, in *Solid State Physics*, edited by F. Seitz and D. Turnbull (Academic, New York, 1956).
[13] I. P. Pen'kov and I. A. Safin, Dokl. Akad. Nauk 156, 139 (1964) [Sov. Phys.-Dokl. 156, 459 (1964)].
[14] Crystals were obtained from the Smithsonian Institution and from Wards Mineral House. These samples originated in Turkey, Romania, Nevada, and Utah.
[15] H. Bayer, Z. Phys. 130, 227 (1951).
[16] N. Morimoto, Mineral J. (Sapporo) 1, 160 (1954).
[17] R. Zallen, M. L. Slade, and A. T. Ward, Phys. Rev. B 3, 4257 (1971).
[18] A. A. Vaipolin and C. A. Porai-Koshitz, Fiz. Tverd. Tela 5, 246 (1963); 5, 256 (1963); 5, 683 (1963) [Sov. Phys.-Solid State 5, 178 (1963); 5, 186 (1963); 5, 497 (1963)].
[19] P. C. Taylor, S. G. Bishop, and D. L. Mitchell, Phys. Rev. Lett. 27, 414 (1971).
[20] I. G. Austin and E. S. Garbett, Philos. Mag. 23, 17 (1971).
[21] J. P. Mathieu and H. Poulet, Bull. Soc. Fr. Mineral. Crystallogr. 93, 532 (1970).
[22] G. Lucovsky and R. M. Martin, J. Non-Cryst. Solids 8–10, 185 (1972).
[23] S. V. Nemilov, Fiz. Tverd. Tela 6, 1375 (1963) [Sov. Phys.-Solid State 6, 1075 (1964)].
[24] C. H. Townes and B. P. Dailey, J. Chem. Phys. 17, 782 (1949).
[25] L. Pauling, *The Nature of the Chemical Bond* (Cornell U. P., Ithaca, N.Y., 1972).
[26] R. Bershon, J. Chem. Phys. 20, 1505 (1952).
[27] C. Dean, Phys. Rev. 96, 1053 (1952).
[28] J. H. Van Vleck, Phys. Rev. 74, 1168 (1948).
[29] A. Abragam and K. Kambe, Phys. Rev. 91, 894 (1953).
[30] A. Abragam, *The Principles of Nuclear Magnetism* (Clarendon, Oxford, England, 1961), p. 110.
[31] M. Bloom, E. L. Hahn, and B. Herzog, Phys. Rev. 97, 1699 (1955).
[32] I. J. Lowe and R. E. Norberg, Phys. Rev. 107, 46 (1957).

[33]E. D. Shaw, Phys. Rev. B 2, 2746 (1970).
[34]K. R. Jeffrey and R. L. Armstrong, Phys. Rev. 174, 359 (1968).
[35]S. Alexander and A. Tzalmona, Phys. Rev. 138, A 845 (1965).
[36]E. A. Kravchenko, S. A. Dembovski, A. P. Chernov, and G. K. Semin, Phys. Status Solidi 31, K19 (1969).
[37]J. Van Kranendonk, Physica (Utr.) 20, 781 (1954).
[38]R. L. Armstrong and K. R. Jeffrey, Can. J. Phys. 47, 2165 (1968).
[39]R. J. Kobliska and S. A. Solin, Phys. Rev. B 8, 756 (1973).
[40]R. Zallen (private communication).
[41]V. Bermudez, J. Chem. Phys. 57, 2793 (1972).
[42]P. C. Taylor, S. G. Bishop, D. L. Mitchell, and D. Treacy, *Proceedings of the Fifth International Conference on Amorphous and Liquid Semiconductors* (Garmisch-Partenkirchen, Germany, 1973).
[43]T. E. Hopkins, R. A. Pasternak, E. S. Gould, and J. R. Herndon, J. Am. Chem. Soc. 753 (1962).
[44]A. J. Leadbetter, A. C. Wright, and A. J. Apling, in *Amorphous Materials*, edited by R. W. Douglas and B. Ellis (Wiley, New York, 1972).
[45]E. A. Porai-Koshits and A. A. Vaipolin, Fiz. Tverd. Tela. 2, 1656 (1960) [Sov. Phys.-Solid State 2, 1500 (1960)].
[46]S. Tsuchihashi and Y. Kawamoto, J. Non-Crystl. Solids 5, 286 (1971).
[47]A. L. Renninger and B. L. Averbach, Phys. Rev. B 8, 1507 (1973).
[48]B. T. Kolomiets and V. P. Pozdnev, Fiz. Tverd. Tela 2, 28 (1960) [Sov. Phys.-Solid State 2, 23 (1961)].
[49]K. Ueberreiter and H. Northmann, Koll. Z. 123, 84 (1951).
[50]R. E. Drews, R. L. Emerald, M. L. Slade, and R. Zallen, Solid State Commun. 10, 293 (1972).
[51]R. Zallen, R. E. Drews, R. L. Emerald, and M. L. Slade, Phys. Rev. Lett. 26, 1564 (1971).
[52]M. M. Mestagh, W. E. Stone, and J. J. Fripiat, J. Phys. Chem. 76, 1220 (1972).
[53]R. C. Zeller and R. O. Pohl, Phys. Rev. B 4, 2029 (1971).
[54]R. B. Stephens, Phys. Rev. B 8, 2896 (1973).
[55]B. Golding, J. E. Graebner, B. I. Halperin, and R. J. Schutz, Phys. Rev. Lett. 30, 223 (1973).
[56]S. Hunklinger, W. Arnold, S. Stein, R. Nava, and K. Dransfield, Phys. Lett. A 42, 253 (1972).
[57]P. C. Taylor, S. G. Bishop, and D. L. Mitchell, Solid State Commun. 8, 1783 (1970).
[58]U. Strom and P. C. Taylor, in Ref. 42.
[59]R. Shuker and P. W. Gammon, Phys. Rev. Lett. 25, 222 (1970).
[60]P. Flubacher, A. J. Leadbetter, T. A. Morrison, and B. P. Stoicheff, J. Phys. Chem. Solids 12, 53 (1957).
[61]W. A. Phillips, J. Low Temp. Phys. 7, 351 (1972).
[62]J. Haupt and W. Müller-Warmuth, Z. Naturforshg. 239, 208 (1968).
[63]J. Haupt and W. Müller-Warmuth, Z. Naturforshg. 249, 1066 (1969).
[64]J. Haupt, Proceedings of the Sixteenth Colloque Ampere, Bucharest, 1970, (unpublished), p. 630.
[65]M. Rubinstein, H. Resing, and J. R. Hendrickson, Bull. Am. Phys. Soc. 19, 202 (1974).
[66]E. L. Hahn, Phys. Rev. 80, 580 (1950).
[67]G. R. Holzman, J. H. Anderson, and W. Koth, Phys. Rev. 97, 542 (1955).
[68]J. Jackle, Z. Phys. 257, 212 (1972).
[69]D. Ng and R. J. Sladek, in Ref. 42.
[70]N. Bloembergen, E. M. Purcell, and R. V. Pound, Phys. Rev. 73, 679 (1948).
[71]J. Hatton and B. V. Rollin, Proc. Phys. Soc. A 199, 222 (1949).
[72]J. A. Sussmann, Phys. Kondens. Materie. 2, 146 (1964).
[73]A previous calculation of the irregular pyramidal molecule by Grechishkin [V. S. Grechishkin, J. Structural Chem. USSR 6, 193 (1965)] is in error due to incomplete orthogonalization of the hybrid wave functions.